NASA Technical Memorandum 79142

INCREASED CAPABILITIES OF THE 30-cm DIAMETER Hg ION THRUSTER

Vincent K. Rawlin and Charles E. Hawkins
Lewis Research Center
Cleveland, Ohio

Prepared for the
Conference on Advanced Technology for Future Space Systems
sponsored by the American Institute of Aeronautics and Astronautics
Langley, Virginia, May 8-11, 1979

INCREASED CAPABILITIES OF THE 30-cm DIAMETER Hg ION THRUSTER

by Vincent K. Rawlin and Charles E. Hawkins

National Aeronautics and Space Administration
Lewis Research Center
Cleveland, Ohio

INTRODUCTION

Several studies have indicated the benefits of using electric propulsion for Large Space Systems (LSS) (Refs. 1 to 3). The magnitude of those benefits depends heavily on the characteristics of the electric propulsion system. Depending on the time frame of a proposed LSS mission, the assumed propulsion system characteristics may range from those of the 30-cm diameter Hg ion thruster system (Refs. 4 and 5) to those of advanced inert gas thruster systems (Ref. 3).

Use of todays thruster technology for planning far-future missions may be overly conservative, while use of advanced technological assumptions probably contains uncertainties in areas such as lifetime.

In general, future energetic missions, using electric propulsion systems, will benefit from any technological advances which allow reductions of the input power, thrust system mass, mission cost, or thrusting time. The realization of such advances implies, to first order (Ref. 6) propulsion systems with thrusters operated at higher thrust density than attainable with present designs.

The Extended Performance Solar Electric Propulsion Thrust System Study (EPSEP, Ref. 7) used a modified Engineering Model Thruster (EMT, Refs. 4 and 5) to produce a maximum thrust per thruster of 0.210 N at a specific impulse of 4850 seconds and an input power of 6465 watts. The standard EMT produces a thrust of 0.129 N at a specific impulse of 2904 seconds for an input power of 2650 watts (Ref. 5). The EMT was modified slightly to increase its lifetime and is now referred to as the Solar Electric Propulsion (SEP) baseline thruster. The major modifications included the use of small hole accelerator grids (SHAG) which allowed the discharge voltage to be reduced from 36 to 32 volts. The combination of SHAG and the reduced discharge voltage resulted in reduced thruster internal erosion with no loss of thruster performance.

For any ion thruster the maximum thrust which may be obtained for a given beam power occurs when that thruster is operated at the maximum beam current and minimum beam voltage. High values of beam current imply large values of total accelerating voltage. The maximum thrust then occurs at operation at the lowest possible value of the ratio of net to total accelerating voltage (R). Reference 8 described the sensitivity of beam divergence to and the limitations of R as a function

cf two-grid accelerator geometry. References 9 and 10 presented the operation of three grid ion acceleration systems and indicated their use resulted in reductions of ion beam divergence and minimum R, when compared to that of two grid thruster operation.

This paper describes the results, to date, of the program to evaluate the operation of the 30 cm mercury ion thruster at increased values of beam current with two and three grid optics. Comparisons with the baseline concepts are made in areas of performance and lifetime.

APPARATUS

A 30 cm diameter laboratory thruster, functionally equivalent to the EMT, was tested with four different ion accelerating systems. The four grid sets used are described in Table 1 which also shows the basic properties of the EMT grids used in Refs. 4, 5, and 7.

The operation of grid sets A and B were compared to show the impact of the addition of a third, or decelerator grid. Each set used the same screen and accelerator grids with each grid mounted on a molybdenum ring at the grid perimeter. The third or decelerator grid (set B) was originally a screen grid from a different grid set. That set had been dished inward, and the screen grid hole pattern was, therefore, not reduced to "compensate" for hole misalinement due to dishing and spacing. As a result, the holes in the accelerator and decelerator grids of set B were nearly co-linear. In addition, the radii of curvature were slightly different (because they were dished at different times) which gave a spacing of about 1 mm at the center for an edge spacing of 0.5 mm. Thus, the results of thruster operation with three grid optics, presented herein probably do not represent the full benefits of this concept.

The decelerator grid was mounted to, but electrically isolated from, the accelerator grid mounting ring and was electrically connected to neutralizer common potential.

Grid set C was identical to grid set A with the exception of the diameters of the accelerator holes. The central region of the grid had 1.27 mm diameter holes while those holes located more than half radius outward were 1.02 mm diameter. This grid set was used to evaluate thruster lifetime at higher beam current.

Grid set D was identical to grid set A with the exception of a thinner accelerator grid and the use of a light-weight mounting ring assembly (Ref. 4). Grid set D is identical to those presently used on the baseline SEP "J" series thruster. The performance of these grids was compared with that of grid set B.

The grids used in the EPSEP study were identical to those of the EMT (Ref. 4) and differed from grid set A in that a larger grid spacing was used, the light-weight mounting system was employed, and the accelerator grid holes were larger in diameter.

Four thermocouples were used to measure thruster component temperatures. One was on the cathode orifice plate, another on the screen grid mounting ring, and two on the thruster anode. The anode thermocouples were positioned 1.9 and 6.8 cm, respectively, from the downstream end of the anode along a line parallel to the thruster axis.

Three beam edge ion probes were used to analyze variations of the ion beam divergence as functions of grid geometry and extraction voltages. Reference 8 describes the details of these probes which have an approximate collection area of 0.35 cm^2 and were used as retarding potential analyzers. The probes were positioned along a line parallel to the thruster axis at a radial location such that the probe centers were located at angles of 52°, 65°, and 81°, respectively, from the outer most grid holes.

Laboratory type power supplies (Ref. 5) were used and an optical spectrometer (Ref. 11) was employed to obtain spectrol line intensities of the propellant atoms and ions and sputtered discharge chamber component atoms.

All of the tests were conducted in a 0.9 m diameter bell jar of the 7.6 m diameter by 21.4 m long vacuum tank at the Lewis Research Center.

RESULTS AND DISCUSSION

The results of tests, conducted to evaluate 30 cm mercury ion thruster operation with two and three grid ion optics at higher values of beam current are presented and compared with those of the baseline SEP and EPSEP thrusters which used conventional two grid optics.

Ion Optics

Perveance. - The performance of the ion accelerating system is measured by its ability to efficiently collimate and accelerate the ion beam. Figure 1 shows the maximum beam current obtained as a function of the total accelerating voltage for grid sets A, B, and D. Based on these data, the maximum beam current (for 30 cm diam Hg thrusters) obtainable with these grids is given by the following equation:

$$J_{B_{MAX}} = \frac{1.7\times10^{-6}\, V_T^2}{\ell^2} \qquad (1)$$

where

JB_{MAX} maximum beam current, amps

V_T total accelerating voltage, volts

ℓ effective accelerating distance, mm

The effective accelerating distance is defined here as the sum of the screen grid thickness, the cold grid to grid spacing, three-fourths of the acceleration grid thickness, and the change in grid to grid spacing during operation. This expression was used in Ref. 12 to correlate a large quantity of data from many different geometries of dished grids for 30 cm mercury ion thrusters. For grids dished outward, the change in grid-to-grid spacing was estimated to be about -0.26 mm (Ref. 12). Most of this change in spacing was believed to occur soon after initiation of the thruster discharge. The different slopes for the data of Fig. 1 are probably due to the addition of the third grid for set B and the different mounting system used on grid set D. These differences, as well as discharge power variations as the beam current was varied, probably had second order effects on the grid-to-grid spacing.

Equation (1) was obtained over ranges of beam current, total voltage, and cold grid spacing of; 1 to 6.2 amperes, 1000 to 3000 volts, and 0.56 to 0.88 mm, respectively. The minimum value of ℓ to be used in Eq. (1) is expected to be about 0.9 mm for 30 cm diameter dished grids. Sovey (Ref. 13) presented a similar expression for 8 and 30 cm diameter ion thrusters using closely spaced two grid dished optics with argon, xenon, and mercury propellant. Over the range of data obtained by Sovey, his expression and Eq. (1), are in good agreement.

For normal thruster operation with some operating margin, total accelerating voltages of about 200 volts higher than those predicted by Eq. (1) are required. The maximum value of the total accelerating voltage is determined by electrical breakdowns between the grids. For closed spaced grids, this value is in excess of 5000 v/mm and does not affect operation in voltage ranges of interest.

Ratio of net-to-total acclerating voltage, R. - The range of R governs the range of specific impulse over which a thruster may be operated. For a given grid set, operating at any beam current and total voltage, the ion beam divergence increases as the net ion beam voltage or R decreases. The upper limit of R occurs when the accelerator grid voltage is too low in magnitude to prevent electrons from the neutralized ion beam from flowing upstream into the thruster. For SHAG optics the maximum value of R is about 0.9 (Ref. 8). The lower limit of R is determined by a rapid increase in accelerator grid current due to the impingement of poorly focussed ions. For two grid optics the minimum value of R (R_{MIN}) is in the range of 0.5 to 0.7 (Ref. 8). For a beam current of 5 amperes, the perveance limit of a grid set (Eq. (1), operated at R equal to 0.5, requires the beam and accelerator voltages to be about +1000 volts and -1000 volts, respectively. Severe erosion of the downstream side of the accelerator grid by change exchange ions would be ex-

pected from extended operation at this condition. However, the addition of a third grid or decelerator, downstream of the accelerator grid, has been found to allow thruster operation at lower values of R (Ref. 10). Figure 2 shows the percentages of accelerator and decelerator currents, with respect to the beam current, for two and three grid optics as functions of R. These currents are due to primary ion and change exchange ion impingement. R_{MIN}, for the three grid system, was found to be about 0.2 indicating a beam voltage as low as 400 volts is possible for Hg ion beam current of 5 amperes. Figure 2 also shows that the use of a decelerator reduces the accelerator impingement current, probably by acting as a shield to low energy charge exchange ions as well as improving the focussing of thrust ions. The current collected by the decelerator grid was also a small fraction of the beam current. The percentages shown were nearly independent of variations of beam current and total voltage.

The trends of R shown in Fig. 2 for two and three grid optics are also expected to be independent of propellant type. Therefore, because specific impulse varies inversely with the square root of the propellant atomic mass, the lowest allowable value of specific impulse will increase as the propellant atomic mass is decreased.

In Ref. 8 the ion beam edge divergence from two grid optics was reported to increase as the accelerator grid hole diameter was decreased. Figure 3 shows that for two grid optics the beam edge divergence increased, for R equal to 0.6, from 58° to 77° as the accelerator grid hole diameter was decreased from 1.52 to 1.14 mm. Figure 3 also shows the improved focussing effects of the SHAG optics with a decelerator grid. The addition of a decelerator grid to two grid SHAG optics reduced the beam divergence to that of the EMT two grid optics. The beam edge angle increased for both grid configurations as R was decreased, however, the effect was slightly less for three grid optics. The results of Fig. 3 were also found to be independent of beam current variations.

Discharge Chamber

Higher thruster power densities imposes new requirements not only on ion optics performance but also upon the discharge chamber performance. Operation of the discharge chamber is characterized by performance parameters such as discharge propellant utilization efficiency, η_{UD}; discharge power per beam ampere, ϵ_I; lifetime parameters such as component erosion rates; and steady-state temperatures of components such as the cathode, anode and ion optics. These parameters were found to be independent of the use of a decelerator grid and, for SHAG optics, were dependent on beam current, discharge voltage, or discharge current.

Performance. - Figure 4 shows ϵ_I as a function of η_{UD} (corrected for doubly charged ions) for various beam currents and discharge voltages. The η_{UD} was found to increase with beam current at constant discharge voltage. However, the

fraction of multipy charged ions also increases leading to reductions of the thrust and thruster lifetime. Based on the results of Ref. 11, the thruster was also operated at a lower discharge voltage to reduce the erosion of discharge chamber components, such as the screen grid, particularly at higher beam currents. Figure 4 shows the expected reduction in discharge chamber efficiency as the discharge voltage was reduced.

Lifetime. - The useful life of an ion thruster is presently limited by sputtering erosion of discharge chamber components by discharge ions. Reference 11 has shown that thruster component erosion rates may be correlated with the spectral emission from eroded component atoms. The spectral intensity is a complex function of the atom density and the exciting electron density and temperature. In addition, the molybdenum (Mo) atom density has two sources: the screen grid and accelerator grid. It was assumed that most of the signal is from screen grid erosion.

Figure 5 shows the variation of the normalized spectral line intensity for Mo as functions of the discharge voltage for different values of beam current. At constant values of discharge voltage and beam current the intensity was found to increase linearly with cathode emission current. To eliminate the effects of emission current variations as the discharge voltage and beam current were varied, the observed Mo intensities were divided by the cathode emission current at each point. Figure 5 shows that, at constant beam current, the normalized Mo intensity decreased rapidly with discharge voltage until that voltage reached 32 volts at which point the intensity became relatively insensitive to further reductions in discharge voltage. However, at any discharge voltage, the Mo line intensity increased with beam current. Spectral line intensities for singly, doubly, and triply charged mercury ions showed trends similar to those of Fig. 5. Based on Fig. 5 and other data, an extended test of a thruster operated at a 3 ampere beam current was conducted using grid set C. Table 2 compares thruster and facility operating conditions as well as screen grid erosion rates for the 3 ampere test and the baseline SEP and EPSEP thrusters. Accounting for the effects of facility pressure on thruster erosion (Ref. 11), the erosion rates expected in space for each thruster operating condition are about equal. Thus, thruster lifetime may be held constant, as ion beam current density is increased, if techniques to reduce the sputtering rate, such as reduction of the discharge voltage, are employed. Attempts to greatly reduce the discharge voltage through variations of physical baffle diameter, magnetic baffle current and cathode flow rate, as the beam current was increased, were thwarted. The minimum discharge voltage was found to be about 26 volts and further variations in the thruster parameters, mentioned above, resulted in discharge voltage increases. Measurable spectral intensity signals from multiply charged mercury ions still exist at 26 volts, possibly because of the inherent peaked plasma density profile of the divergent magnetic field thruster.

Discharge chamber geometries having more uniform plasma distributions, such as those in multipole designs (Refs. 14 and 15), may be required to permit further reductions of discharge voltage and thruster internal erosion at elevated beam currents.

Temperatures. - Thruster operation at high values of beam current, at near constant ϵ_I and discharge voltage, implies high values of discharge power, cathode emission current, and thruster component temperatures. Cathode, anode, and screen grid mounting ring temperatures are plotted in Fig. 6 as functions of the discharge current collected by the anode. Of the latter three components the downstream end of the anode was the hottest, approaching 500° C, because most of the current is collected at that end of the anode in a divergent magnetic field thruster. The temperature of the anode, at a location 5 cm upstream of the electron collection region, was about 120° C cooler than the downstream end. A multipole magnetic field thruster, which has a more uniform plasma density, is less likely to have such large temperature gradients. The temperature of the grid mounting ring, which is attached to the downstream end of the thruster, is also shown in Fig. 6. It increased with discharge current and this variation was typical for both types of grid mounting rings tested. The mounting ring temperatures (°C), for a given discharge current were about half the value of the downstream anode temperature.

The cathode tip temperature, at constant cathode flow rate, increased nearly linearly with discharge current at about 15° C per ampere. The temperature was also noted to be a strong function of cathode flow rate, increasing about 60° C as that flow rate was increased from 80 to 160 mA equivalent. Higher cathode temperatures, expected at higher values of emission current, can probably be reduced with modest increases in the cathode orifice diameter as suggested in Ref. 16.

Thruster Performance

Table 3 shows the performance, obtained in this study, for thrusters operated with three grid optics. Performance was calculated using measured input parameters and thrust loss factors obtained from estimated values of beam divergence (Ref. 17) and doubly charged ions (Ref. 18). Figure 7 presents the maximum values of thrust as a function of specific impulse (lowest beam voltage) for a thruster with three grids and compares them to those of the baseline SEP and EPSEP thrusters. The curvature, at decreasing values of specific impulse, occurs because the propellant utilization efficiency decreases with decreasing beam current thereby decreasing the specific impulse. The major point of Fig. 7 is that, over the range of SEP specific impulse variation, the use of three grid optics allows several times more thrust per thruster at any value of specific impulse. In addition, the ratio of the maximum thrust from the three grid thruster to the thrust of the SEP thruster increases with specific impulse.

Figure 8 shows the thrust as a function of thruster power for a thruster with three grid optics and for the SEP and EPSEP thrusters. The use of three grid

optics allows as much as 24 percent more thrust than the SEP thruster (at 2650 W input power) and nearly 75 percent more thrust than the EPSEP thruster (at 3 kW). These increases in the thrust to power ratio occur because the three grid optics were operated at a lower specific impulse as shown in Fig. 7. This does require an increase in the propellant mass fraction, for a given mission, if no other changes are made. But the use of three grid optics, at these values of specific impulse and input power, allows thruster operation at a beam voltage approximately equal to expected solar array bus voltages.

Thrusters (8, 15, and 30 cm diam) have been operated (Refs. 19 to 21, respectively) with most of the thruster power supplied directly from a solar array (direct drive). The major stated uncertainty in the application of that concept is the possibility of interactions between the high voltage solar array and the space and thruster generated plasmas. Present power processors for SEP are designed to operated from solar arrays with output voltages as high as 400 volts and negligible plasma interactions. Results of this investigation have indicated that, through the use of three grid optics, beam voltages as low as 400 volts at beam currents up to 5 ampere are possible. Therefore, is appears that direct drive is possible and that about 95 percent of the thruster input power (beam and discharge powers) may be obtained directly from the solar array. This would result in considerable savings in system cost and mass through reductions in the requirements for power processing, waste heat radiators, and solar array power.

All of the data in Table 3 are plotted in Fig. 9 which shows that the efficiency of a given thruster as a function of specific impulse is nearly independent of beam current. This occurs because decreases in the unionized propellant mass losses are offset by increases in the thrust losses due to multiply charged ions as the beam current is increased.

Also shown in Fig. 9 is the performance of the SEP and EPSEP thruster over their power throttle range. The use of three grid optics not only increases the range of thruster operation at low values of specific impulse over that possible with two grid optics (about 30 percent), but also increases the thruster efficiency at values of specific impulse less than about 2800 seconds. This efficiency increase is due to the improved ion focussing characteristics of three grid optics over the entire range of specific impulse.

At low values of specific impulse the power required to create the beam ions is comparable to the output beam power thereby reducing the power efficiency to less than 50 percent. The use of other discharge chamber designs, such as that of Ref. 14 which employs magneto-electrostatic containment of ions and electrons, offers potential discharge power reductions of about 25 percent which would result in thruster efficiencies about 6 percent greater than those of Fig. 9 at a specific impulse of about 2000 seconds.

CONCLUSIONS

A 30-cm diameter mercury ion thruster, using two and three grid ion accelerating systems, was operated at increased values of beam current. When a third, or decelerating grid, was added to the conventional two-grid optics of a SEP-like thruster, the ion beam focussing properties were found to improve as expected from theoretical considerations. This improvement not only extended the range of thruster operation at low values of specific impulse but allows several times more thrust than SEP or EPSEP baseline thrusters at any specific impulse. In addition, the total thruster efficiency, as a function of specific impulse, is increased for values of specific impulse from 1200 to 2800 seconds. The use of three grid optics at low values of specific impulse may also enable the direct use of solar array power for about 95 percent of the thruster input power thereby reducing the propulsion system cost and mass through reductions of power processor requirements.

Thruster discharge chamber performance was unaffected by the addition of the decelerator grid.

The lifetimes of discharge chamber components as functions of beam current and discharge voltage were inferred from spectroscopic analysis of the thruster discharge. Reduced component erosion appears possible if techniques such as reducing the discharge voltage are employed to reduce the quantity and energy of ions which do sputter damage. Results of an extended test, conducted at an increased beam current of 3 amperes and a reduced discharge voltage of 28 volts, predict a thruster lifetime, at space conditions, which is no less than that of the baseline SEP thruster.

REFERENCES

1. "Initial Technical, Environment, and Economic Evaluation of Space Solar Power Concepts," Vol. I - Summary, NASA TM X-74309, 1976, and Vol. II - Detailed Report, NASA TM X-74310, 1976.

2. Stearns, J. W., "Large-Payload Earth-Orbit Transportation with Electric Propulsion," Jet Propulsion Laboratory, Pasadens, Calif., TM 33-793, Sep. 1976. (NASA CR-148973)

3. Byers, D. C., and Rawlin, V. K., "Electron Bombardment Propulsion System Characteristics for Large Space Systems," NASA TM X-73554, 1976.

4. Masek, T. D., Poeschel, R. L., and Collett, C. R., "Evolution and Status of the 30-cm Engineering Model Ion Thruster," AIAA Paper 76-1006, Nov. 1976.

5. Bechtel, R. T., and Rawlin, V. K., "Performance Documentation of the Engineering Model 30-cm Diameter Thruster," AIAA Paper 76-1003, Nov. 1976.

6. Masek, T. D., MacPherson, D., Gelon, W., Kami, S., Poeschel, R. L., and Ward, J. W., "Advanced Electrostatic Ion Thruster for Space Propulsion," Hughes Research Labs., Malibu, Calif., Apr. 1978. (NASA CR-159406)

7. Poeschel, R. L. and Hawthorne, E. I., "Extended Performance Solar Electric Propulsion Thrust System Study, Vol. 1, Executive Summary," Hughes Research Labs., Malibu, Calif., Sep. 1977 (NASA CR-135281-Vol. 1).

8. Rawlin, V. K., "Sensitivity of 30-cm Mercury Bombardment Ion Thruster Characteristics to Accelerator Grid Design," AIAA Paper 78-668, Apr. 1978.

9. Meadows, G. A., and Free, B. A., "Effect of a Decel Electrode on Primary and Charge-Exchange Ion Trajectories," AIAA Paper 75-427, Mar. 1975.

10. Aston, G., and Kaufman, H. R., "Ion Beam Divergence Characteristics of Three-Grid Accelerator Systems," AIAA Paper 78-669, Apr. 1978.

11. Rawlin, V. K. and Mantenieks, M. A., "Effect of Facility Background Gases on Internal Erosion of the 30-cm Mercury Ion Thruster," AIAA Paper 78-665, Apr. 1978.

12. Rawlin, V. K., Banks, B. A., and Byers, D. C., "Design, Fabrication, and Operation of Dished Accelerator Grids on a 30-cm Ion Thruster." AIAA Paper 72-486, Apr. 1972.

13. Sovey, J. S., "A 30-cm Diameter Argon Ion Source," AIAA Paper 76-1017, Nov. 1976.

14. Ramsey, W. D., "12 cm Magneto-Electrostatic Containment Mercury Ion Thruster Development," AIAA Paper 71-692, June 1971.

15. Longhurst, G. R. and Wilbur, P. J., "1" cm Multipole Mercury Ion Thruster," AIAA Paper 78-682, Apr. 1978.

16. Kaufman, H. R., "Technology of Electron-Bombardment Ion Thrusters," Advances in Electronics and Electron Physics, Vol. 36, Academic, New York, 1974, pp. 265-373.

17. Danilowicz, R. L., Rawlin, V. K., Banks, B. A., and Wintucky, E. G., "Measurement of Beam Divergence of 30-Centimeter Dished Grids," AIAA Paper 73-1051, Oct. 1973.

18. Poeschel, R. L., "High Power and 2.5 kW Advanced Technology Ion Thrusters," Hughes Research Labs., Malibu, Calif., Feb. 1977 (NASA CR-135163).

19. Stover, J. B., "System Tests with Electric Thruster Beam and Accelerator Directly Powered from Laboratory Solar Arrays," NASA TM X-3353, 1976.

20. Sater, B. L., "The Advantages of the High Voltage Solar Array for Electric Propulsion," AIAA Paper 73-1103, Oct. 1973.

21. Gooder, S. T., "Operational Compatibility of 30-Centimeter-Diameter Ion Thruster with Integrally Regulated Solar Array Power Source," NASA TN D-8428, 1977.

TABLE 1. - ION OPTICS DESCRIPTION

Grid set	Number of grids	Screen grid		Accelerator grid		Decelerator grid	
		Hole diam, mm	Thickness, mm	Hole diam, mm	Thickness, mm	Hole diam, mm	Thickness, mm
A	2	1.91	0.38	1.14	0.51	----	----
B	3	1.91	0.38	1.14	0.51	1.91	0.38
C	2	1.91	0.38	1.27/1.02	0.51	----	----
D (SEP)	2	1.91	0.38	1.14	0.38	----	----
EMT (EPSEP)	2	1.91	0.38	1.52	0.51	----	----

TABLE 2. - SCREEN GRID EROSION RATES

Thruster	Grid set C	SEP	EMT and EPSEP
Beam current, amp	3.0	2.0	2.0
Discharge voltage, V	28	32	36
Discharge losses per beam amp, W/A	192	192	198
Facility pressure, Torr	4×10^{-7}	2×10^{-7}	2×10^{-7}
Screen grid erosion rate, nm/hr	5.5±2.6	9±2.5	8±1.3

TABLE 3. - THRUSTER PERFORMANCE (GRID SET B)

Beam current, amp	Beam voltage, V	Accelerator voltage, V	Discharge voltage, V	Discharge losses per beam ampere, W/A	Measured propellant utilization efficiency	Thrust loss factor[a]	Ratio of net to total accelerating voltage	Thruster input power, W	Thrust, N	Specific impulse, sec	Thruster efficiency
1.0	785	100	32	224	0.880	0.964	0.87	1094	0.055	2378	0.586
	585	300	↓	↓	↓	↓	.65	894	.048	2053	.540
	385	500	↓	↓	↓	↓	.43	694	.039	1666	.459
	185	700	↓	↓	↓	↓	.21	494	.027	1155	.309
2.0	1185	200	32	192	.911	.955	.85	2854	.134	2997	.689
	885	500	↓	↓	↓	↓	.63	2254	.116	2590	.653
	585	800	↓	↓	↓	↓	.42	1654	.094	2106	.586
	285	1100	↓	↓	↓	↓	.20	1054	.066	1470	.451
3.0	1485	300	28	197	.920	.956	.83	5161	.225	3392	.725
	1185	600	↓	↓	↓	↓	.66	4261	.201	3030	.700
	885	900	↓	↓	↓	↓	.49	3361	.174	2619	.664
	585	1200	↓	↓	↓	↓	.33	2461	.141	2129	.598
	385	1400	↓	↓	↓	↓	.21	1861	.115	1727	.523
4.0	1485	400	28	198	.943	.948	.78	6862	.298	3448	.734
	1185	700	↓	↓	↓	↓	.62	5662	.266	3080	.709
	985	900	↓	↓	↓	↓	.52	4862	.243	2808	.688
	785	1100	↓	↓	↓	↓	.41	4062	.217	2507	.656
	485	1400	↓	↓	↓	↓	.26	2862	.170	1970	.573

[a]Estimated values from Refs. 17 and 18.

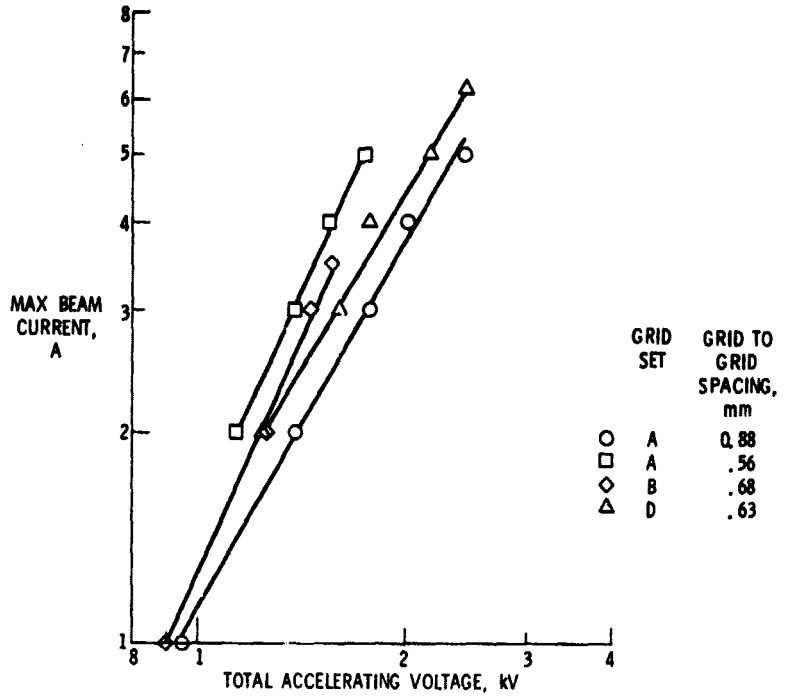

Figure 1. - Maximum beam current as a function of total accelerating voltage.

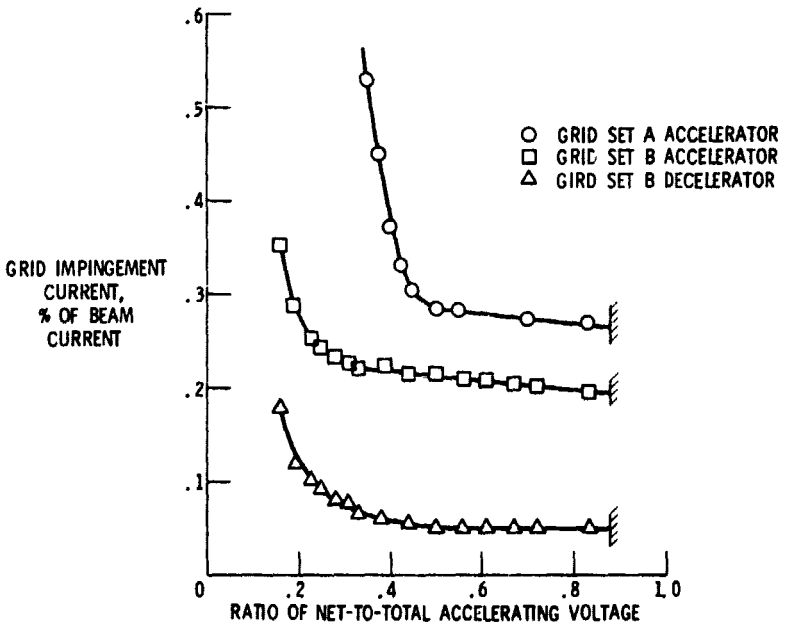

Figure 2. - Grid impingement current as a function of R, beam current = 2.0 A.

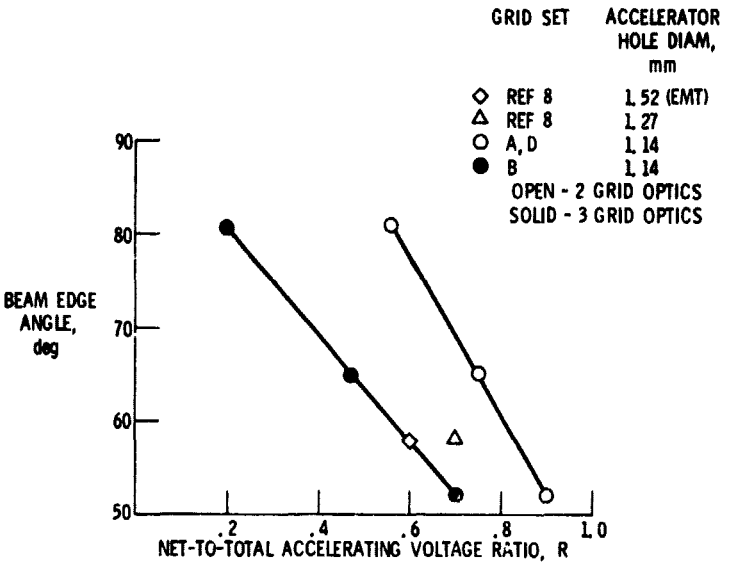

Figure 3. - Beam edge angle as a function of R, beam current = 2.0 A.

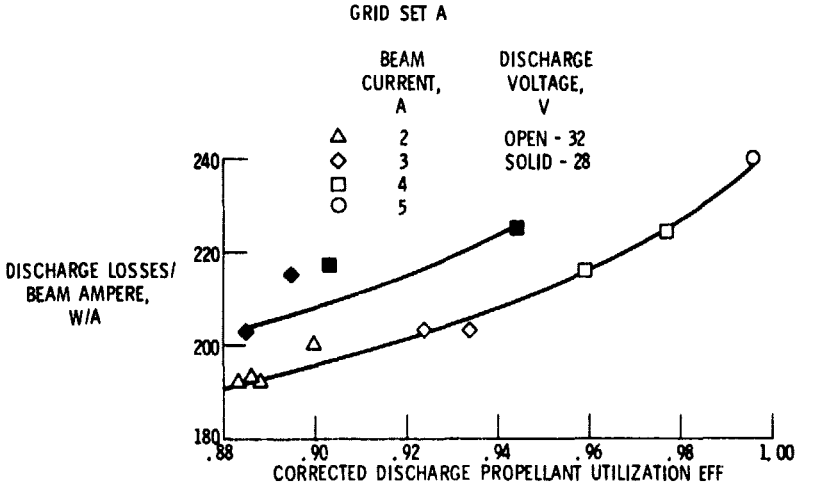

Figure 4. - Discharge losses as a function of discharge propellant utilization efficiency (grid set A).

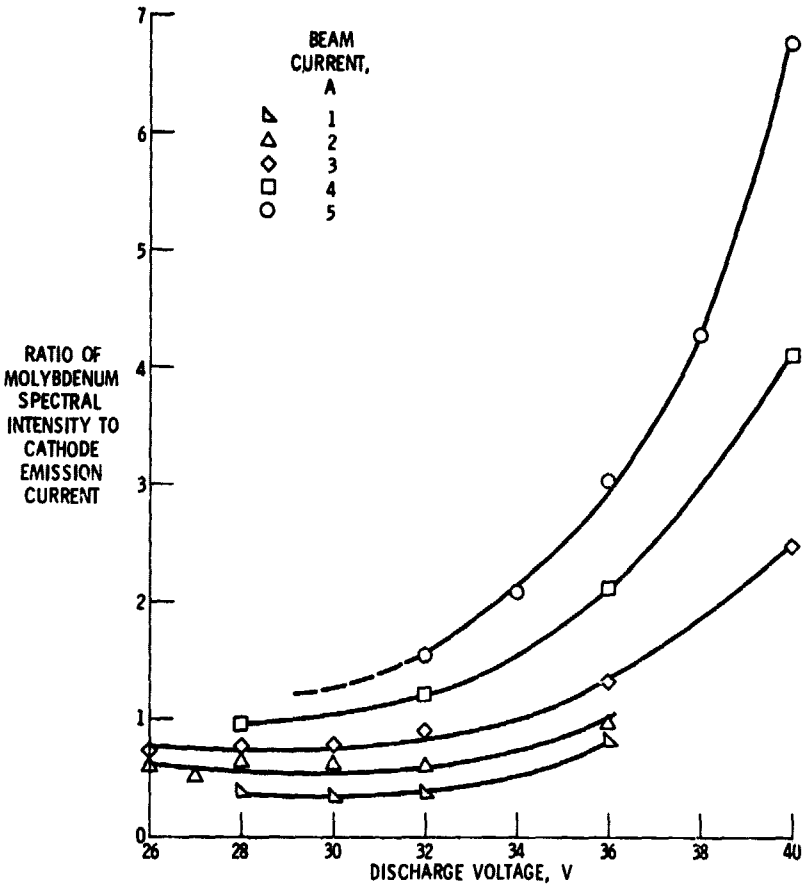

Figure 5. - Normalized Mo intensity as a function of discharge voltage (grid set A).

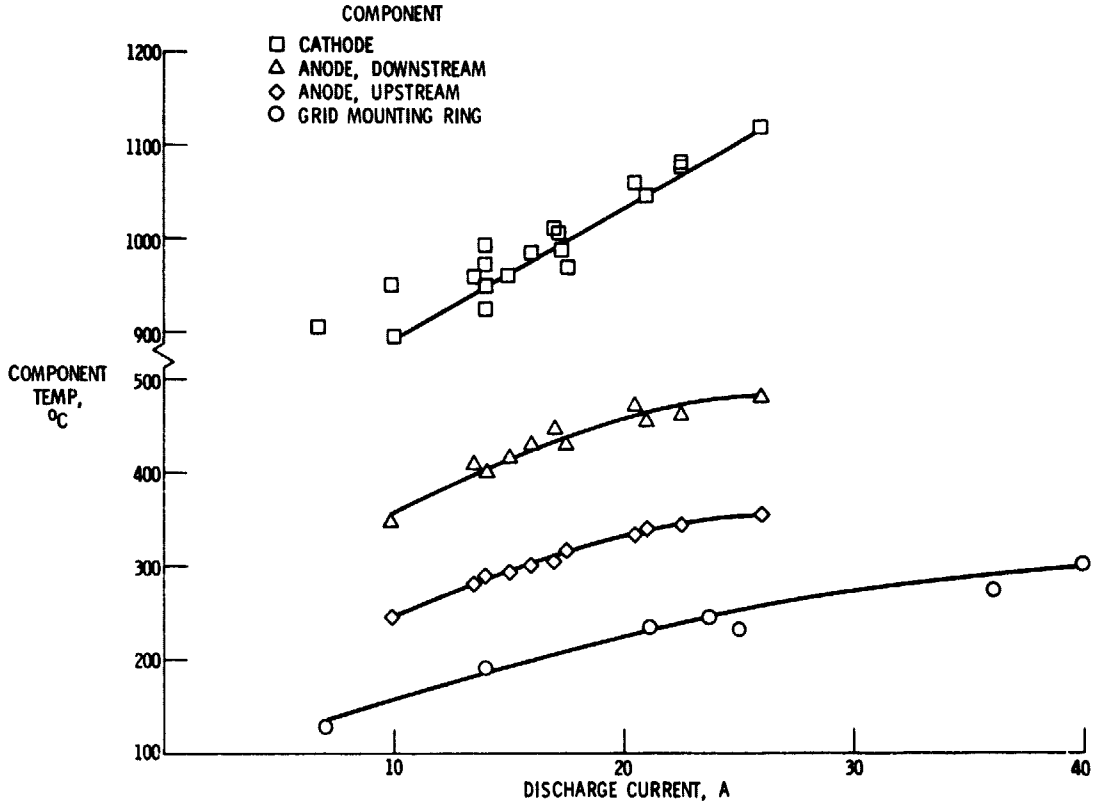

Figure 6. - Thruster component temperatures as functions of discharge current.

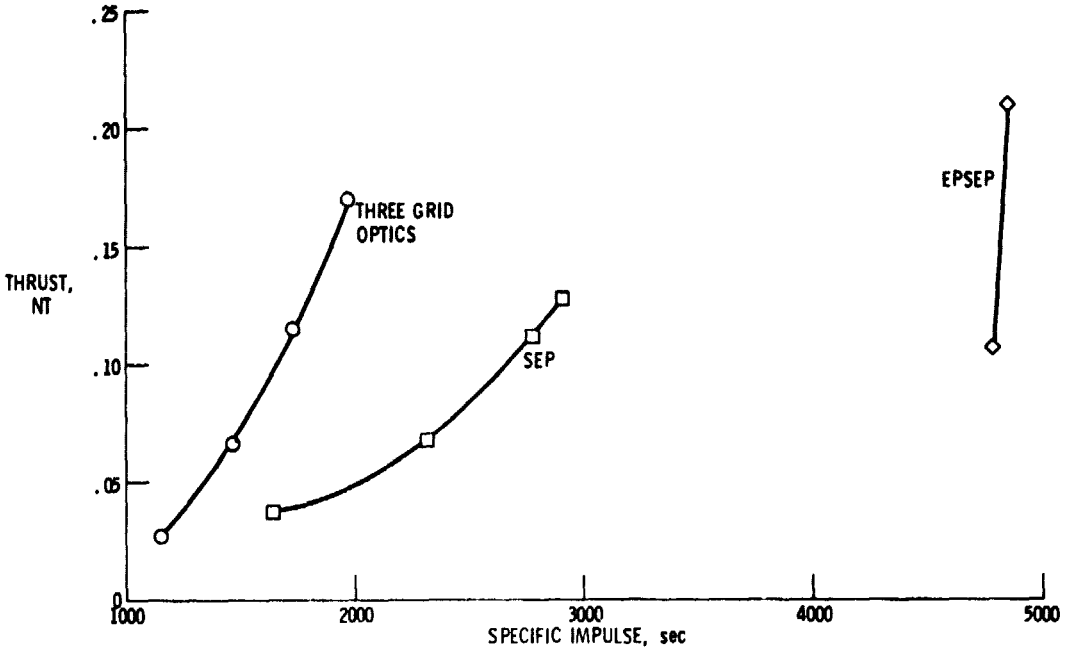

Figure 7. - Demonstrated maximum thrust as a function of specific impulse.

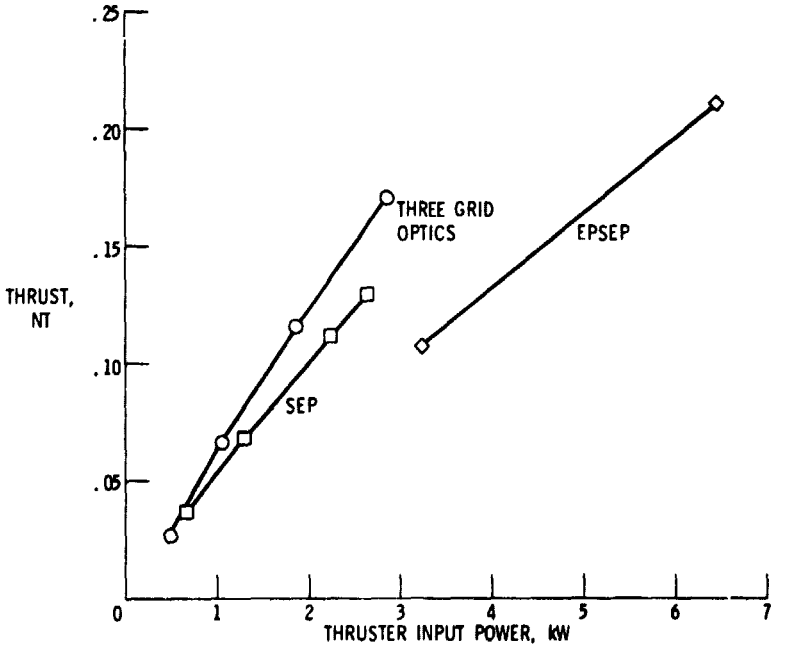

Figure 8. - Demonstrated maximum thrust as a function of thruster input power.

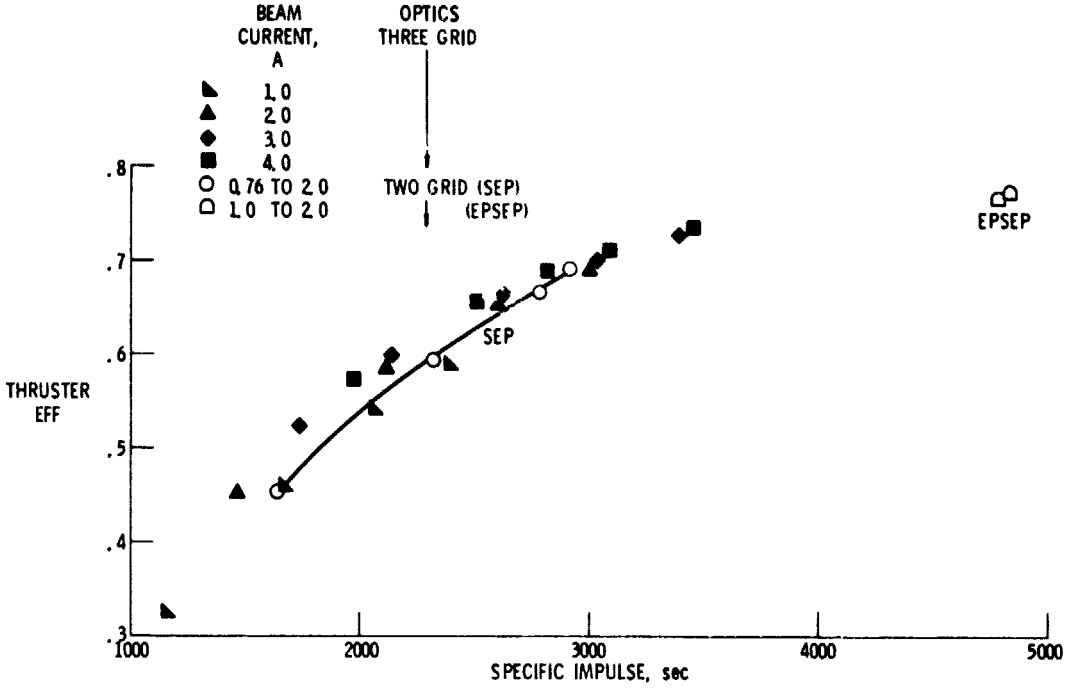

Figure 9. - Thruster efficiency as a function of specific impulse.